ISA Transactions, Volume 120, January 2022, pp.55-69
DOI:10.1016/j.isatra.2021.03.003

A simple active carbody roll scheme for hydraulically actuated railway vehicles using internal model control

Egidio Di Gialleonardo[a,*], Matteo Santelia[a], Stefano Bruni[a], Argyrios Zolotas[b]

[a] *Dipartimento di Meccanica, Politecnico di Milano, Via La Masa, 1 I-20156 Milan, Italy, e-mail: egidio.digialleonardo@polimi.it, stefano.bruni@polimi.it, matteo.santelia@polimi.it*
[b] *Centre for Autonomous and Cyber-Physical Systems, SATM, Cranfield University, Cranfield, MK43 0AL, UK, e-mail: a.zolotas@cranfield.ac.uk*

[*] Corresponding author

Graphical Abstract

Tilting Rail vehicle with novel hydraulic actuation

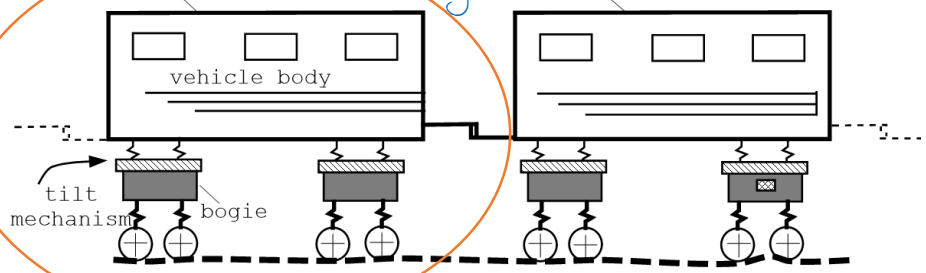

A simple tilt controller to enable

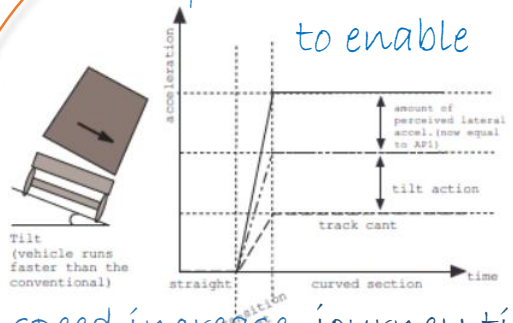

speed increase, journey time reduction, passenger ride quality

Implementation/validation (in-house rail software tool)

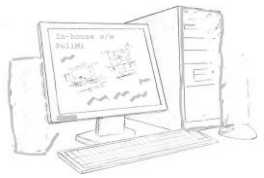

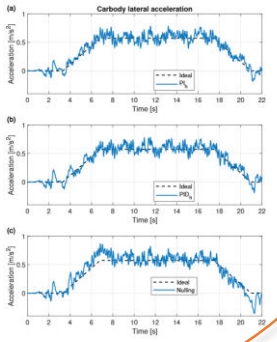

Controller	Comfort evaluation				
	P_{CT} [%]	$\max(\ddot{\varphi})$ [rad/s]	$\max(\ddot{y})$ [m/s²]	$\max(\ddot{y})$ [m/s³]	$RMS(\ddot{y})$ [m/s²]
PI_t	2.468	**0.031**	0.664	0.217	0.195
PI_h	2.158	0.032	0.634	0.212	0.199
PID_t	**1.993**	0.033	0.619	**0.207**	**0.194**
PID_h	2.006	0.034	**0.599**	0.224	0.203
Nulling	3.465	**0.031**	0.740	0.251	0.204

Control analysis and design

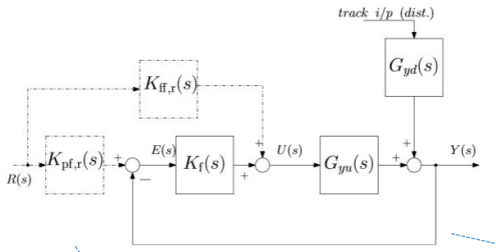

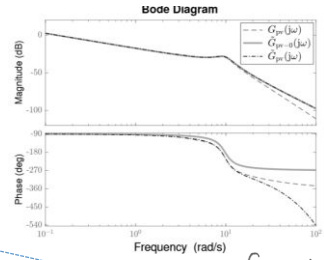

$$\tilde{G}_{pv}(s) = \frac{k' e^{-\tilde{\theta} s}}{s(\tau_2^2 s^2 + 2\xi_2 \tau_2 s + 1)}$$

Simplify (model for control)

for two types of tilt: preview and nulling

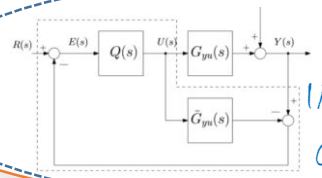

simple IMC-based controller

Model it

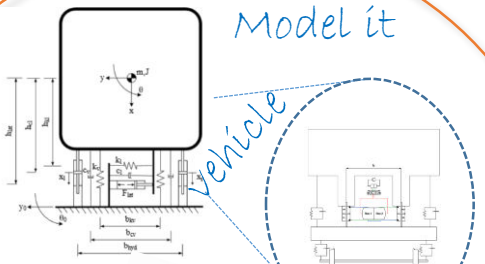

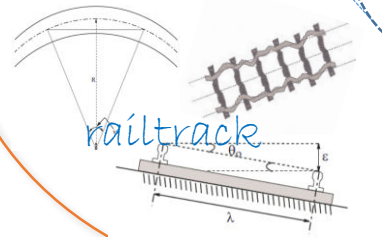

Highlights

- The first classical internal model control (IMC) design in the context of railway carbody roll control is presented.
- A simple control approach for a recent vehicle concept, that offers limited carbody roll with hydraulic actuation, is proposed.
- The control design provides a model simplification process that facilitates PI and PID-type control structures without the need for complex optimization.
- Performance of preview and nulling-type tilt setups are compared.
- Vehicle roll performance is studied on the deterministic (curving acceleration response) and stochastic (ride quality) trade off.

A simple active carbody roll scheme for hydraulically actuated railway vehicles using internal model control

Abstract

The paper presents the first classical internal model control (IMC) design in the context of railway carbody roll control. We propose a simple control approach for a recent hydraulically actuated vehicle body roll concept that offers limited carbody roll. The IMC approach addresses both preview- and nulling-type tilt setups, highlighting related benefits and limitations. The design provides a model simplification process that facilitates PI and PID-type control structures without the need for complex optimization. A simple, yet practical, tool for the industrial rail rolling stock engineer in vehicle control design is offered. Vehicle roll performance is rigorously studied on the deterministic (curving acceleration response) and stochastic (ride quality) trade off. Simulations are performed on an in-house multibody dynamics software package employing a realistic nonlinear railway vehicle model and allow to appropriately assess the performance of preview and nulling type tilt performance. The results obtained confirm that preview tilt control offers the better tilt performance as it utilises a tilt command reference, and highlighted that nulling-type tilt performance remains at a relatively comparable level with the former.

Keywords: railway vehicle, carbody roll, internal model control, preview control, hydraulic actuation, PID control

1. Introduction

Tilting trains lean the body of the vehicle inwards on curves to reduce the lateral acceleration experienced by the passengers. Train speed increases through the curve, resulting to journey time reduction. From a practical point of view, active control is used to perform the tilting actions and active tilting train system is an area whereby control engineering has been a major

contributor to modern railway vehicle technology [1, 2]. Nowadays a large number of modern high speed trains incorporate a form of tilt [3, 4].

A review of tilting body systems for trains is provided in [5]. Passive tilt was used in early implementations, using a an arrangement where the secondary suspension (i.e. the suspension stage connecting the car body to the bogie frames) are raised above the car body's centre of mass creating a pendulum effect. This solution however reduces significantly the space available for passengers and the tilt angle in curve transitions cannot be controlled effectively, impairing ride quality.

Nowadays, most tilting body implementations use a tilting bolster, allowing to produce relatively large rotations of the car body (in the range of 6-8 degrees).Recently, direct tilt obtained through the active control of the secondary suspension (i.e. the suspension stage connecting the car body to the bogie frames) has been proposed. This implementation, although only allowing a limited amount of car body tilt (in the range of 1-2 degrees) is simpler and lighter compared to the bolster-based one, so it is particularly appropriate for very-high speed trains with service speeds above 300 km/h, which are subject to severe constraints in terms of weight and space.

One method to achieve direct tilt is to actively inflate / deflate the air springs in a pneumatic secondary suspension [6, 7, 8], but this solution has significant drawbacks in terms of increase of air consumption ans also in relation to the low pass-band of the air springs used as actuators. More recently, a concept based on an active anti-roll bar formed by cross-connected hydraulic actuators as proposed [9]. This concept removes the drawbacks of the active air springs, but keeps the advantages compared to tilting-bolster designs in terms of lower weight and space use. This latter solution is considered in this paper, with the aim of defining simple but effective tilt controllers.

Initial studies of controllers for active tilting trains used feedback control from a lateral accelerometer mounted on the body of the vehicle, but it proved difficult to achieve a sufficient quickness of response on the transitions at the start and end of curves without causing a deterioration of ride quality on straight track. Most tilting train implementations now use a command-driven system in which a signal from an accelerometer on a non-tilting part of the previous vehicle indicates the required tilting angle, with a straightforward tilt angle feedback controller locally ensuring that each vehicle tilts to the commanded angle [2]. This is commonly known as 'precedence' tilt - the advanced information enables a sufficient level of filtering to be applied to remove the effect of track irregularities on the tilt command signal.

Such a control scheme is quite complex; amongst other things it must reconfigure when the train changes direction, and it is also difficult to provide a satisfactory performance for the leading vehicle of the train. Recent advances enabled the tilt preview (command) signal to be obtained from track databases and/or GPS however the overall concept remains similar.

In fact, simple tilt related control design is still of interest to the railway community [10]. Although tilt action could be used to provide an increase in passenger comfort at conventional vehicle speeds, the main commercial benefit from using tilting vehicle technology is the reduction of journey times on conventional railtracks without degrading passenger comfort. For information on ride comfort within the remit of railway vehicles and in particular tilting trains, the interested reader is referred to [11].

This paper is the first, to the best knowledge of the authors, that presents classical Internal Model Control (IMC) design considerations in the context of railway active suspensions and in particular of carbody roll motion control. Internal Model Control (IMC) is a well known inverse-based systematic controller design framework which aims to provide a suitable trade-off between designed system performance and robustness [12]. It is based on, what is known as, Q-parametrization (or Youla parametrization) of all stabilizing controllers for a given system [13, 14, 15]. Its use as an alternative to the classical feedback structure to obtain controllers satisfying practical robustness and performance makes it very appealing. This is the exact feature exploited in this paper for carbody active roll control. The model used for the design of the controllers is in first approximation a simple integrating plant, as it will be shown in section 3.2. A certain number of papers related to IMC based PID controller design for integrating systems are already available in literature [16, 17, 18], however not in the context of active suspensions in railway field.

2. Methodology and structure of the paper

The design of simple and robust controllers for car body roll in railway vehicles is still an open issue and is critical to shorten travel times at the same time ensuring proper ride quality and avoiding motion sickness for passengers. The design of controllers also depends on the specific technology chosen for tilt actuation, and not much work has been previously published regarding control strategies for hydraulic tilt actuation.

This paper proposes an approach based on the use of Internal Modal Control to design simple and robust tilt controllers. The performance of the controllers is then assessed using a realistic simulation tool which allows to consider the effect of both deterministic and random features of the railway track.

2.1. Methodology

The methodology followed in this paper is based on three main steps. Firstly, a simplified linear model of the railway vehicle is derived. The model considers the car body, secondary suspensions (i.e. the suspension stage connecting the car body to the bogie frames) and the hydraulic actuation system realising the tilt function. This model neglects some features of the railway vehicle which are not essential to the synthesis of the controller, particularly wheel/rail contact and the effect of primary suspension (i.e. suspensions connecting the wheelsets to the bogie frames), resulting in relatively simple plant transfer functions suitable for the synthesis of the controllers.

The second step consists of the synthesis of controllers. Different choices are made here, to compare a less aggressive controller to a more aggressive one and to assess the performance of nulling-type controller to preview controllers, see Section 3.2 for more details.

Finally, the different controllers are assessed using a software for the multi-body simulation of railway vehicles, developed in-house at the Department of Mechanical Engineering of Politecnico di Milano [19, 20, 21]. This software incorporates a detailed non-linear model of wheel/rail contact, allowing to consider in full the effect of deterministic and stochastic track inputs, see Section 2.2. The multi-body model of the vehicle used for the assessment of the controllers considers a complete vehicle with four wheelsets, two bogies and one car body. Primary and secondary suspensions are considered in full detail, so that the effect of modelling errors involved with the simplified vehicle model used in the controller design phase can be evaluated.

2.2. Vehicle excitation track inputs

The operational scenario utilizes deterministic rail track information, for simulation and performance assessment, of a typical Italian high-speed network with: cant elevation 105 mm, maximum curve radius $R_{\max}$ = 5500 m, transition length of 330 m at each end of the track corner. Provision of limited carbody tilt is considered (as is the case for such a vehicle structure), with

maximum tilt angle on steady-corner of $\approx 2\,\text{deg}$ (which offers $\approx 14\%$ speed increase to 340 km/h). In fact, this is equivalent to $\approx 37.5\%$ tilt compensation on steady-curve in the case of (non-preview) partial-nulling.

Stochastic track irregularities are included in the model as a random spatial realisation of a power spectral density (PSD) defined in ERRI B176 report [22]. Such track elements normally are difficult to measure (some information can be provided from a monitored track database, or a specialist track condition measurement vehicle), while attempts to estimate using vehicle-based sensor exist in the current literature [23]. The track irregularity PSD, in this work, is actually based on measured irregularity data referred to as "Low Level", which can be representative of track defects on high-speed lines.

2.3. Structure of the paper

This paper is organized as follows: Section 3 derives the simplified linear model used for the synthesis of controllers. In section 4 the tilt control design setup is described. In section 5 the tilt-targeted Internal Model Control (IMC) design is presented. Section 6 presents results of the proposed control strategies tested on the non-linear multi-body model, and conclusions on the presented work are drawn in Section 7.

3. Vehicle modeling for control

3.1. Lumped parameter model

The reference vehicle used in this work has a typical architecture made up of one carbody and two bogies, each one equipped with two wheelsets. The layout of the suspensions has been modified in order to include active capabilities by means of an active roll device. The working principle of the device, when operated in passive mode, is based on hydraulically interconnected suspensions [24] nominally providing zero stiffness in vertical direction and a non-zero roll stiffness. Other applications of hydraulic interconnected suspensions are available in literature, exclusively related to the automotive field [25, 26, 27]. A scheme of the layout of the device is shown in Figure 1 for one bogie and includes the following main components:

- two linear hydraulic actuators, placed on the two sides of the bogie and connecting the bogie frame with the carbody;

- a main hydraulic circuit (green and blue lines in the figure), cross-connecting the chambers of the actuators. Two additional reservoirs (Res 1 and Res 2) are introduced in the circuit;
- a feeding hydraulic circuit (red lines in the figure) controlling fluid flow in the reservoirs through a pump and a servo-valve in order to operate the device in active mode.

In addition, an active lateral element (in the form of a simple "hold-off" device [28]) is used to maintain the centered position of the carbody during curve negotiation. This essentially prevents the carbody to make contact with the suspension bumpstops, while keeping the vehicle within the prescribed gauge and also reducing the load transfer effect related with the lateral movement of the carbody. The reader may find more details on the functioning of the device and its dimensioning in [9].

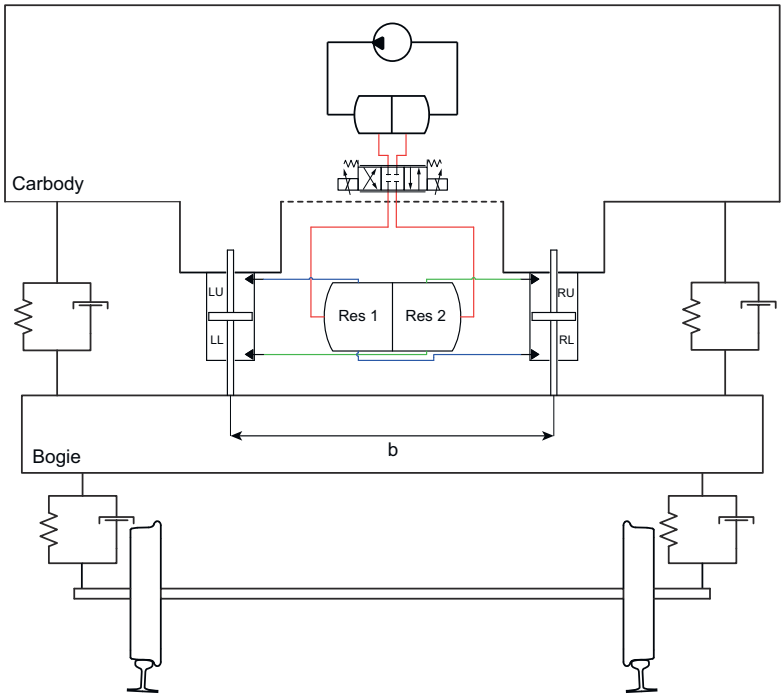

Figure 1: Layout of the hydraulic circuit for roll actuation

In order to facilitate appropriate control strategies for active carbody roll action, a lumped parameter model of the vehicle is defined. The model

comprises six states, i.e. four of which describe the lateral and roll motions of the vehicle body, and another two states characterizing the dynamics of the hydraulic system that provides roll actuation. The schematic diagram of Figure 2 illustrates the lumped parameter model of the vehicle with hydraulic tilt actuation. The model consists of a rigid body (i.e. carbody) resting on a conventional suspension and on two hydraulic actuators realizing tilt actuation. The suspension employs two pneumatic springs that act in the vertical direction and a linear spring-dash pot element representing the lateral stiffness of the suspension. The force generated by the active lateral device is defined in an open loop sense based on measuring the non-compensated lateral acceleration of the carbody:

$$F_{\mathrm{lat}} = m\left(\frac{v^2}{R} - g\theta_0\right) \tag{1}$$

with m being half the mass of the carbody, v the speed of the vehicle, R the radius of the curve and θ_0 the track cant. It is important to remark that in general the mass is a varying parameter related to the number of passengers or to the payloads, but in this work the worst case of the car body mass at full payload is considered.

The model shown in Figure 2 utilizes two independent coordinates i.e. y and θ to describe the lateral movement and roll rotation of the carbody respectively and the values of the vehicle parameter are listed in table B.1. The following set of second-order equations applies

$$m\ddot{y} + c_{\mathrm{l}}\dot{y} - c_{\mathrm{l}}h_{\mathrm{cl}}\dot{\theta} + k_{\mathrm{l}}y - k_{\mathrm{l}}h_{\mathrm{kl}}\theta = F_{lat} \tag{2}$$

$$\begin{aligned} J\ddot{\theta} - c_{\mathrm{l}}h_{\mathrm{cl}}\dot{y} + \left(c_{\mathrm{l}}h_{\mathrm{cl}}^2 + 2c_{\mathrm{v}}\frac{b_{\mathrm{cv}}^2}{4}\right)\dot{\theta} - k_{\mathrm{l}}h_{\mathrm{kl}}y + \left(k_{\mathrm{l}}h_{\mathrm{kl}}^2 + 2k_{\mathrm{v}}\frac{b_{\mathrm{kv}}^2}{4}\right)\theta = \ldots \\ \ldots b_{\mathrm{hyd}}A_{\mathrm{p}}\Delta P - F_{\mathrm{lat}}h_{\mathrm{lat}} - c_{\mathrm{l}}h_{\mathrm{cl}}\dot{y_0} + \left(c_{\mathrm{l}}h_{\mathrm{cl}}^2 + 2c\frac{b_{\mathrm{cv}}^2}{4}\right)\dot{\theta_0} - k_{\mathrm{l}}h_{\mathrm{kl}}y_0 \end{aligned} \tag{3}$$

The vertical displacement of the body's centre of gravity is not included in the model because that motion is decoupled from the considered (lateral, roll) motion components, due to the symmetry of the passive suspension elements and the cross-connection between the actuators of the roll device

In addition, the hydraulic actuation model is defined on the basis of the following assumptions:

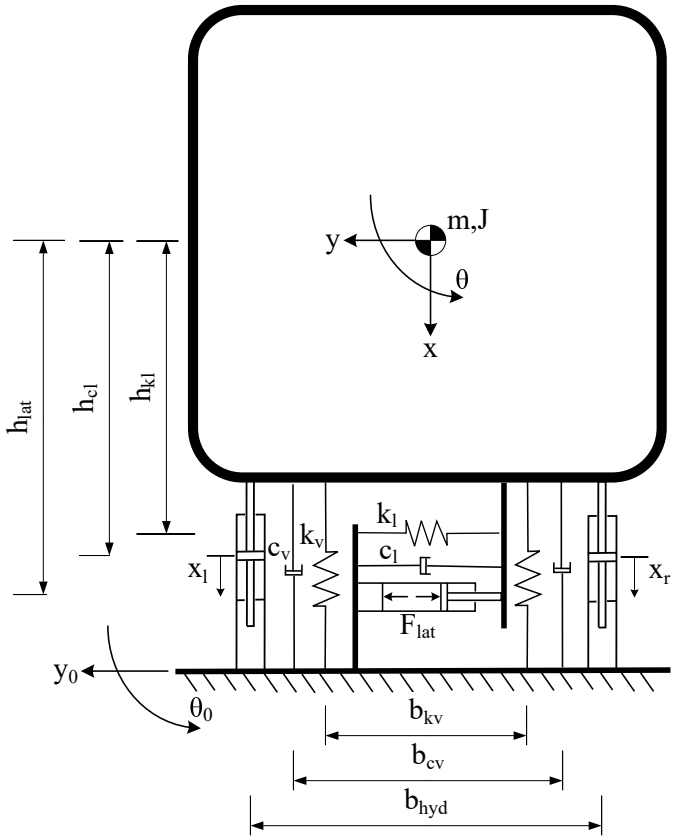

Figure 2: Lumped parameter model of the vehicle

- isothermal conditions of the fluid;
- partially compressible fluid in the actuator chambers and reservoirs;
- constant values for the supply and return pressures;
- servo-valve assumed to behave as a 1st order system;
- the pressure differences between two chambers of both cylinders are the same (i.e. loss in the pipes are neglected) $\Delta P_\mathrm{l} = -\Delta P_\mathrm{r} = \Delta P$.

The aforementioned assumptions result in a single state equation describing the dynamics of the hydraulic tilt actuation system [29], i.e.

$$\frac{V_0}{\beta}\Delta\dot{P} + \left(2C_\mathrm{i} + C_\mathrm{e}\right)\Delta P + A_\mathrm{p}\left(\dot{x}_\mathrm{l} - \dot{x}_\mathrm{r}\right) = Q \tag{4}$$

with $\dot{x}_\mathrm{l}$ and $\dot{x}_\mathrm{r}$ representing the speed of the hydraulic pistons on the left and right side of the carbody respectively, V_0 is half of the volume of each branch of the circuit including the additional reservoir, see Figure 1, C_i and C_e the internal and external leakage coefficients and A_p the piston area. Q is the semi-difference of the flow rates in the two chambers of each piston which is related to the position of the servo-vale spool x_s by the linearized equation

$$Q = k_\mathrm{q} x_\mathrm{s} - k_\mathrm{c} \Delta P \tag{5}$$

For small values of the carbody roll (tilt) angle, the speed of the left and right pistons can be expressed as function of the carbody roll rate according to the following linearized kinematic relationships

$$\dot{x}_\mathrm{l} = \dot{\theta} b_\mathrm{hyd} \; ; \quad \dot{x}_\mathrm{r} = -\dot{\theta} b_\mathrm{hyd} \tag{6}$$

Combining equations (4), (5) and (6) yields the following first-order state equation for the hydraulic tilt actuation system

$$\frac{V_0}{\beta} \Delta \dot{P} + \left(2C_\mathrm{i} + C_\mathrm{e} + k_\mathrm{c}\right) \Delta P + A_\mathrm{p} b_\mathrm{hyd} \dot{\theta} = k_\mathrm{q} x_\mathrm{s} \tag{7}$$

Finally, a simplified first-order model is introduced to represent the dynamics of the servo-valve spool, i.e.

$$\dot{x}_\mathrm{s} + \frac{1}{\tau_\mathrm{s}} x_\mathrm{s} = \frac{1}{\tau_\mathrm{s}} u_\mathrm{s} \tag{8}$$

where u_s is the command to the servo-valve and τ_s the time constant of the servo-valve. The values of the hydraulic tilt actuation system parameter are listed in table B.2. Combining equations (2), (3), (7) and (8) presents a linear, sixth order model for the vehicle with hydraulic tilt actuation that can be described in the following state-space matrix form:

$$\dot{\mathbf{x}} = \mathbf{A}\mathbf{x} + \mathbf{B}_\mathrm{u} u + \mathbf{B}_\mathrm{w} \mathbf{w} \tag{9}$$

with state vector, control input vector, and exogenous input vector (associated to the track geometry and stochastic irregularities)

$$\mathbf{x} = \begin{bmatrix} \dot{y} & \dot{\theta} & y & \theta & \Delta P & x_\mathrm{s} \end{bmatrix}^\mathrm{T} ; u = \begin{bmatrix} u_\mathrm{s} \end{bmatrix} ; \mathbf{w} = \begin{bmatrix} \frac{1}{R} & \dot{y}_0 & \dot{\theta}_0 & y_0 & \theta_0 \end{bmatrix}^\mathrm{T} \tag{10}$$

respectively. The state vector comprises lateral $(y, \dot{y})$ and roll $(\theta, \dot{\theta})$ related variables for the vehicle body dynamics, as well as the two hydraulic actuator dynamics variables $(\Delta P, x_s)$. The matrices used for the state space representation and the values of the parameters used for the model are reported in Appendix B.

3.2. Plant transfer functions

Two different control strategies are analysed, the so-called preview- (identified as "pv") and nulling-type tilt (identified as "nln"). The preview-type is based on the a-priori knowledge of the reference signal from track databases and/or GPS. This enables to provide a feed-forward action to the roll device leaving to the feed-back the compensation of model uncertainties and track disturbance. On the other hand, the nulling-type is a simpler version of the controller aiming at nullifying or partially compensating the lateral acceleration felt by the passengers, making use of an acceleration measured on the vehicle itself (hence also referred to as "local-per-vehicle" tilt)[1].

From the state-space model presented earlier, the plant transfer functions representing: (i) the servovalve -to body roll output relationship and (ii) the control command -to the servovalve -to effective cant deficiency output relationship are obtained. The transfer functions are presented below

$$G_{\mathrm{pv}}(s) = \frac{335.1(\mathit{1 + 0.262s + 0.082s^2})}{(\mathbf{1 + 2484s})(1 + 0.046s)(\mathit{1 + 0.235s + 0.084s^2})(1 + 0.038s + 0.0104s^2)} \tag{11}$$

$$G_{\mathrm{nln}}(s) = \frac{335.1(\mathbf{1 - 0.139s})(\mathit{1 + 0.401s + 0.089s^2})}{(\mathbf{1 + 2484s})(1 + 0.046s)(\mathit{1 + 0.235s + 0.084s^2})(1 + 0.038s + 0.0104s^2)} \tag{12}$$

The transfer functions are presented in the form of zero-pole-gain structure displaying time constants. Also, selected terms in equations (11) and (12) are highlighted in boldface or italic to ease recognising some meaningful parts of the plant's dynamics as will be commented later in the paper.

The pole-zero map and the frequency response for the two tilt related transfer functions (11), (12) are shown on Figure 3. The analysis of the pole-zero maps (Figure 3 (a)) illustrates the difference between the two transfer functions, i.e. the presence in the nulling-type tilt of a non-minimum phase (nmp) zero highlighted in the bottom subfigure. The impact of the 'unstable' zero, in the nulling-tilt case, is shown on the Bode plot (Figure 3 (b)) between the transfer functions $G_{\mathrm{pv}}(s)$ (depicted in solid line) and $G_{\mathrm{nln}}(s)$ (depicted in

[1]This can be via accelerometers on the carbody or from accelerometers on the bogie frame (non-tilting part) with the signal appropriately low-pass filtered.

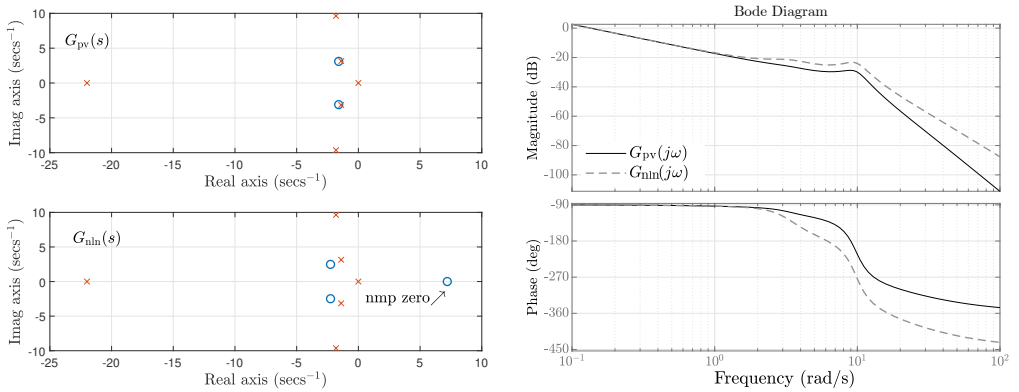

(a) Pole-zero map (b) Bode plot

Figure 3: Uncompensated plant stability and frequency response of $G_{\rm pv}(j\omega)$, $G_{\rm nln}(j\omega)$

dashed line). Clearly, $G_{\rm nln}(s)$ Bode plot exhibits higher magnitude and larger phase lag as frequency increases, compared to $G_{\rm pv}(s)$. This imposes strict control performance constraints in the nulling-tilt case (an issue of main concern in early tilting train applications that ultimately led the industry to adapting the more complex preview- tilt used in tilting trains nowadays [30]). It is noted that both preview and nulling-type tilt design, excited by the same exogenous inputs for appropriate comparison, provide the same amount of tilt angle which results to approximately 14% tilt compensation at the higher speed[2]. For completeness, information on Modal Dominance Index (MDI) [31] is presented to illustrate the most important modes in the system. First a slow-fast decomposition is performed due to the fact that the almost integrating portion of the system (i.e. hydraulic actuator) is dominating the response, i.e. $G_{\rm xx}(j\omega) = G_{\rm xx-s}(j\omega) + G_{\rm xx-f}(j\omega)$ (with the latter term depicting the remaining faster modes of the system, also see [32]). Note that identifier "xx" denotes "pv" or "nln", depending on the case to analyse.

Table 1 presents the Modal Dominance Index (MDI) for both pv and nln plants. One can clearly note that the upper sway mode (first row, at approx 1.56 Hz) shows as the most dominant 'fast' mode in the system (having approx 63% MDI). From the MDI results there is an early indication that

[2]The amount of lesser acceleration felt by passengers of the tilting vehicle compared to that from the non-tilting vehicle at the same high speed.

Poles (fast modes)	MDI (γ) % (pv)	MDI (γ) % (nln)
$-1.813 \pm 9.635j$	62.90	44.81
$-1.391 \pm 3.148j$	23.30	39.87
-21.99	13.80	15.32

Table 1: Modal Dominance Index for $G_{\text{pv}-\text{f}}(j\omega)$, $G_{\text{nln}-\text{f}}(j\omega)$ (faster vehicle modes)

a 3rd order plant transfer function (i.e. almost integrator dynamics plus the most dominant faster mode) approximation for control design seems an appropriate choice[3] as a starting point. Similar MDI analysis is followed for $G_{\text{nln}-\text{f}}(j\omega)$ (with the sequence maintained but the 'local' output for control in model clearly impacts the % dominance per mode, in particular the two first modes are almost sharing dominance).

4. The tilt control design setup

Figure 4 presents a 2-DoF classical feedback control setup framework that accommodates both pv and nln control structures. The (dash-dotted) paths/blocks $K_{\text{ff,r}}(s), K_{\text{pf,r}}(s)$ represent the reference feed-forward and pre-filter blocks respectively (note these apply only in the pv design where a tilt reference command exists). The pv[4] setup represents the industrial-norm in tilting train operation today, whereby the command signal provides the required amount of roll (given from a track database or via GPS or via preview-vehicle sensors) and the feedback signal feeds vehicle body roll information.

In the nulling-type setup the command signal is absent, hence blocks $K_{\text{ff,r}}(s), K_{\text{pf,r}}$ are not utilized, and is only the feedback - the so-called effective cant deficiency for partial tilt - providing the required amount of tilt. Note the effective cant deficiency is constructed by using a portion of the measured lateral acceleration signal (mapped into an equivalent angle) and a portion

[3]Here, MDI is used to present modal importance and an insight on plant simplification.

[4]It is noted that (preview tilt) command-driven tilt with precedence is more complex than nulling-type tilt in terms of signal (vehicle) interconnections, GPS and/or track database information accuracy. Nulling-type is the simpler, more straightforward in terms of fault detection, scheme used in early tilting train technology [30]

of body roll to provide the required partial tilt compensation. In our work, nln with 37.5% tilt compensation provides the same amount of tilt angle as in the pv case.

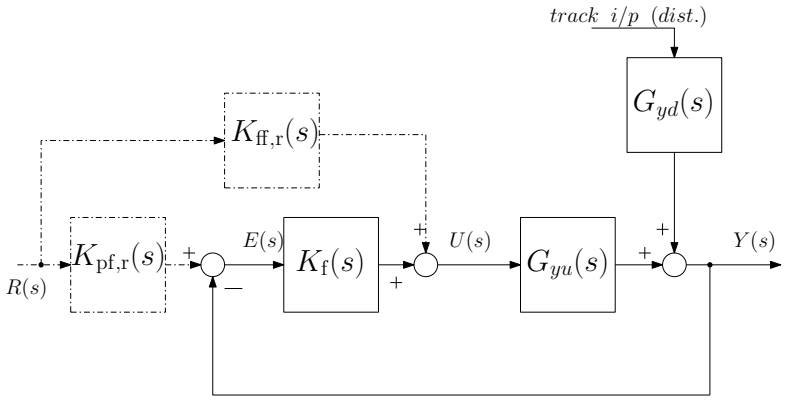

Figure 4: 2-DoF feedback control setup for design purpose

Normally the command (reference) signal is provided with a small preview time (i.e. enabling start of tilt action just before the corner section) but no preview time is utilized here following the same consideration as in [9] for consistency. In addition, non-measurable exogenous input (disturbance) track input information is assumed.

For the case of a reference signal (i.e. in our case the preview tilt control), see Figure 4, the following choices facilitate independent design of $K_{\mathrm{ff,r}}(s)$ (feedforward[5]) and $K_{\mathrm{f}}(s)$ (feedback) controllers [33],[34] respectively,

$$K_{\mathrm{ff,r}}(s) = G_{yu_-}^{-1}(s)F_{\mathrm{r}}(s); \quad K_{\mathrm{pf,r}}(s) = G_{yu_+}(s)F_{\mathrm{r}}(s)$$

where $G_{yu_-}(s)$ is the invertible and $G_{yu_+}(s)$ the non-invertible portions of the plant (the assumption for plant factorisation is $G_{yu}(s) = G_{yu_-}(s)G_{yu_+}(s)$). The portion $F_{\mathrm{r}}(s)$ is included to guarantee properness of the $K_{\mathrm{ff,r}}(s)$ transfer function. Note that, the output signal $Y(s)$ refers to vehicle body roll angle for preview tilt case, and to the effective cant deficiency for the nulling-type tilt case (of course in this case $K_{\mathrm{ff,r}}(s)$=0, $K_{\mathrm{pf,r}}(s)$=0).

[5]We utilise the concept of reference command feedforward rather than disturbance feedforward for simplicity and fair comparison to previous work in [9].

5. Internal Model Tilt-targeted control design

5.1. Internal model Control in a nutshell

Internal Model Control (IMC) is a well known inverse-based systematic controller design framework which aims to provide a suitable trade-off between designed system performance and robustness [12]. Traditionally IMC has been very popular in process control applications especially on tuning complex PID control loops [35, 36, 37]. IMC has been employed in process control examples with time delay [18], as well as applications of feedforward control for disturbance attenuation [38]. Internal Model Control principles have also been studied recently for speed control of nonlinear uncertain heavy duty vehicles [39] (although this is quite different application to the one in this paper). There is a diverse set of IMC formulations i.e. SISO and MIMO formulations [40], Continuous and Discrete-time [41], Linear and Nonlinear approaches [42, 43]. In this paper we mainly concentrate on a SISO control approach viewpoint.

Utilizing plant (model) information in IMC is essential and in plants characterized by complex models model reduction is required. Rivera has rigorously presented perspectives of model reduction within an IMC framework [44] while Skogestad in [45] has presented elegant rules for model reduction and tuning of PID controllers (all in process control industry examples). It is without doubt that many IMC design rules stem from experience/lessons within the process control area. Clearly mechanical (or electro-mechanical) systems, where oscillatory modes arise, present a different challenge compared to process control examples. However, process control inspired rules can be the prelude to more specialised IMC design considerations for more dynamically complex in nature systems typified in the railway vehicle control domain.

In terms of IMC related applications to systems of a suspensions-nature few can be found in the current literature i.e. related to Maglev applications [46], automotive stability control [47, 48], quarter-car model control [49] and references within. However, available papers with some link to IMC for vehicle systems do not extensively discuss on ways of reduction in the design stages and no work directly linked to core IMC approach exists for railway vehicle systems especially in the case of roll motion. This is the area this paper strongly contributes to from an IMC control design viewpoint.

The IMC feedback setup is shown in Figure 5, where G_{yu} is the (actual or realistic) plant and $\tilde{G}_{yu}$ the model. For completeness, we also show the

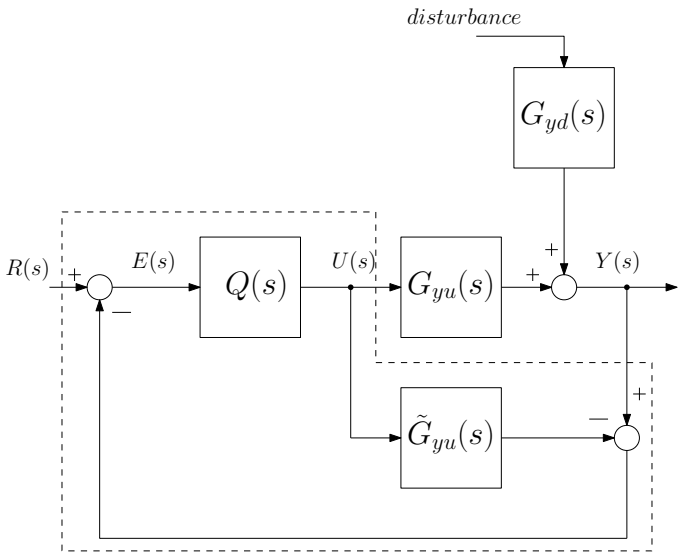

Figure 5: Typical IMC feedback controller framework ($Q(s)$ IMC controller)

disturbance input channel, although it is not used directly in the design as we validate the designed controller on the realistic in-house software. A starting point is to set $\tilde{G}_{yu} = G_{yu}$ although in most cases the model will be an approximation of the true plant. Also note that we are able to design the feedback controller and feed-forward controller portions independently as discussed earlier in the previous section.

The IMC design approach proceeds as follows: Firstly the plant (model) is factorized to a minimum-phase portion (invertible portion) and another portion including non-invertible elements (i.e. non-minimum phase zeros and/or delays), i.e.

$$G_{yu}(s) = G_{yu_+}(s)G_{yu_-}(s) \tag{13}$$

where $G_{yu_-}(s)$ is the minimum-phase and invertible transfer function, while $G_{yu_+}(s)$ contains any nmp zeros of the plant and/or time delays. Then, and based upon the idea of model inverse, the IMC filter $Q(s)$ is chosen as

$$Q(s) = G_{yu_-}^{-1}(s)F(s) \tag{14}$$

$F(s)$ facilitates properness properties of the filter. A simple choice, stems from process control, is $F(s) = \frac{1}{(\tau_f s+1)^n}$ to guarantee properness of $Q(s)$ (via choice of n), with τ_f a tunable time constant for the controller design

(slightly different consideration applies for integrating processes, for example see [50]). We utilize it as a starting design point[6]. The classical feedback controller equivalent (see the dashed box in Figure 5) is given by

$$\begin{aligned} C_f(s) &= Q(s)\left[1 - G_{yu}(s)Q(s)\right]^{-1} \\ &= G_{yu_-}^{-1}(s)F(s)\left[1 - G_{yu}(s)G_{yu_-}^{-1}(s)F(s)\right]^{-1} \\ &= G_{yu_-}^{-1}(s)F(s)\left[1 - G_{yu_+}(s)F(s)\right]^{-1} \end{aligned} \tag{15}$$

Clearly the choice of $F(s)$ adds to the complexity of the feedback controller $C_f(s)$[7]. Under ideal conditions $F(s)$ defines a so-called "model reference" response. Normally $F(s)$ filter considerations that stem from process control examples are initially employed, if these choices do not provide satisfactory results more complex filter dynamics can be used.

5.2. Tilt control-targeted IMC design

Here we discuss modeling considerations for IMC controller, $K_f(s)$ (see Figure 4), design . The pole/zero pairs in the vehicle models as well as the coupled dynamical modes (lateral-roll) may hinder use of simplified models, e.g. that of first or second order dynamics. We show the impact of model structure on controller design and system performance, including discussion on the actuator dynamics contribution. Feedforward action (that applies only in the preview tilt setup) is discussed in the MBS tool implementation.

5.2.1. IMC preview tilt

MDI analysis has provided an insight on model simplification considerations (see vehicle modeling section). Moreover, referring to (11) one can clearly see the lag dominant (almost integrating) mode -introduced by the (linearized) dynamics of the hydraulic actuator- (see bold font in the transfer function) as well as an almost cancelling well-damped complex pole/zero pair (see italic font in the preview tilt plant transfer function (11)).

It is emphasized that the lag dominant mode, introduced by the actuator dynamics, is actually beneficial from an IMC control viewpoint as it facilitates

[6]In the context of oscillatory systems, $F(s)$, can include appropriately damped modes and pole/zero combinations in its structure. This necessitates some designer experience in the application dynamics topic

[7]Note on rational controller form: time delays in (15) are approximated by 1st order Taylor expansion.

substantial plant order simplification. This will ultimately map to a simpler controller design structure.

The PI case: A simple PI type controller is obtained by approximating the original plant model by

$$\tilde{G}_{\mathrm{pv}_1}(s) = \frac{k_1' \mathrm{e}^{-\tilde{\theta}_1' s}}{s} \tag{16}$$

noting the integrating portion and effective delay element in the approximant. The invertible part of (16) is the transfer function excluding the delay. This is a common practice in process control industry whereby delays are naturally arising from the process dynamics/operation, however in the case of electro-mechanical systems as the tilting train the role of the effective delay $\tilde{\theta}_1'$ (in (16)) or $\tilde{\theta}$ (in (19)) is to mainly "correct" the phase profile of the approximate model and is discussed later in this section. The IMC-based PI controller is given by

$$C_{\mathrm{PI}_1}(s) = \frac{1}{k_1' \left(\tau_c + \tilde{\theta}_1'\right)} \left(1 + \frac{1}{4(\tau_c + \tilde{\theta}_1')s}\right) \tag{17}$$

with the integral time constant obtained from simple SIMC (Skogestad IMC) rules [45] (sometimes being referred to as SIMple Control).

$$\tau_I = 4\left(\tau_c + \tilde{\theta}_1'\right) \tag{18}$$

In the PI controller design case, one can clearly see the effect of design parameter τ_c on the integral time constant, (18). In fact, τ_c is the only design parameter to tune in this case. Its initial value is set equal to the given effective delay, i.e. $\tilde{\theta}_1'$ in this case, while increasing it will result to a more robust but slower response.

The simple integrating process approximation of the vehicle model, see (16), is also employed for the feed-forward and pre-filter, i.e. $K_{\mathrm{ff,r}}$, $K_{\mathrm{pf,r}}$ during the preliminary analysis (noting the dominant integrating characteristics of the hydraulic actuator).

The PID-type case: For a PID-type controller a major oscillatory mode should be included in expression (16) (which essentially adheres to the order approximation indication provided by the MDI results presented earlier).

Hence, the approximated plant transfer function is

$$\tilde{G}_{\mathrm{pv}}(s) = \frac{k' \mathrm{e}^{-\tilde{\theta}s}}{s\left(\tau_2^2 s^2 + 2\xi_2 \tau_2 s + 1\right)} \tag{19}$$

It includes dynamics of the upper sway (damping ratio of 18.5%). Figure 6 illustrates the approximated model frequency response (19). Although the magnitude plot of the effective delay-free approximation, indicated as $\tilde{G}_{\mathrm{pv}-0}$, covers the original model magnitude response, clearly a phase error is noted (within the frequency range of the resonance peak). The role of the effective delay $\tilde{\theta}$ is to correct this phase error, and can easily be found graphically. At any frequency ω_{i}, on the frequency response, the time delay error between $G_{\mathrm{pv}}(s)$ and the approximate delay-free model $\tilde{G}_{\mathrm{pv}-0}(s)$ is $\tilde{\theta}(\omega_{\mathrm{i}}) = |\phi_{\mathrm{e}}(\omega_{\mathrm{i}})|\omega_{\mathrm{i}}^{-1}$ ($\phi_{\mathrm{e}}(\omega_{\mathrm{i}})$ is the frequency-dependent phase error between the aforementioned models). To correct the phase error near the maintained resonance mode peak, the effective delay is $\tilde{\theta} = |\phi_{\mathrm{e}}(\omega_{\mathrm{rp}})|\omega_{\mathrm{rp}}^{-1}$ whereby ω_{rp} is the frequency at which the maintained resonance mode peak occurs[8]. In the case of (19) $\tilde{\theta} \approx 0.048$s and $k' = 0.135$, $\tau_2 = 0.102$s, $\xi_2 = 0.185$.

For the approximated plant in (19) the filter[9] is selected as

$$F(s) = \frac{\left(4\tau_0 + \tilde{\theta}\right)s + 1}{\left(\tau_0 s + 1\right)^4} \tag{20}$$

Once again, τ_0 is the single tuning parameter and initially set to $\tilde{\theta}$ (increasing τ_0 provides less aggressive response). Hence, the extended (or filtered) PID controller will be of the form

$$C_{\mathrm{xPID}}(s) = \frac{k_{\mathrm{g}}(\alpha s + 1)(\beta^2 s^2 + \gamma s + 1)}{s(\psi^2 s^2 + \mu s + 1)} \tag{21}$$

Figure 7, compares the Bode plot for the PI controller based on the simple integrating process approximation of the vehicle model, with the PID-type controller (in both cases the manual tuning aimed for not aggressive controller response hence keeping the control sensitivity limited at high frequencies).

[8] an approximation is given by $\omega_{\mathrm{rp}} = \tau_2^{-1}\sqrt{1 - 2\xi_2^2}$ [51].

[9] This stems from process control examples for plant transfer functions higher than 1st order and when typically ramp type inputs need to be addressed [52], [45]. Also, under-damped characteristics in $F(s)$ can be included if needed.

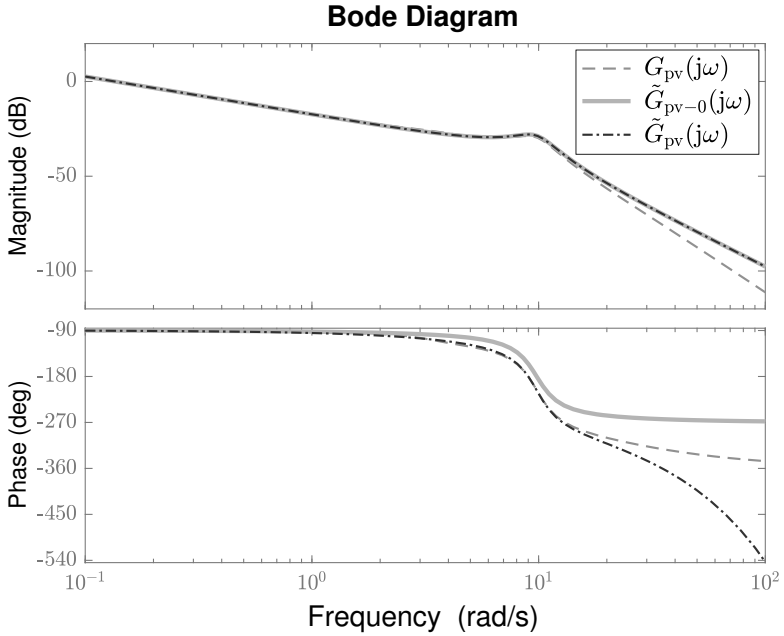

Figure 6: Plant $G_{\mathrm{pv}}(j\omega)$ and its approximations (with and without phase correction $\tilde{\theta}$)

The controller transfer functions are shown in Appendix A (together with applicable remarks). The contribution of the maintained vehicle dynamic modes in the PID-type controller is clearly seen.

Figure 7(b) presents the closed loop magnitude plot. $T(s)$, $S(s)$, $KS(s)$ refer to complementary sensitivity, sensitivity, and control sensitivity transfer functions, respectively. One can clearly see the faster yet robust response facilitated by the PID-type controller.

It is worth mentioning from the results shown on Figure 7(b) that the controllers facilitate a robustly designed system (based on the low peak of the sensitivity transfer functions, as well as the roll off at higher frequency in the complementary sensitivity transfer functions).

5.2.2. IMC nulling-type tilt

The IMC controller design for nulling-type tilt is similar to the process discussed previously (hence extended frequency response results are not presented). The IMC controller is obtained using a simple model similar to (19), however now the effective delay mainly characterises the phase delay introduced by the nmp zero (with no approximation phase error required

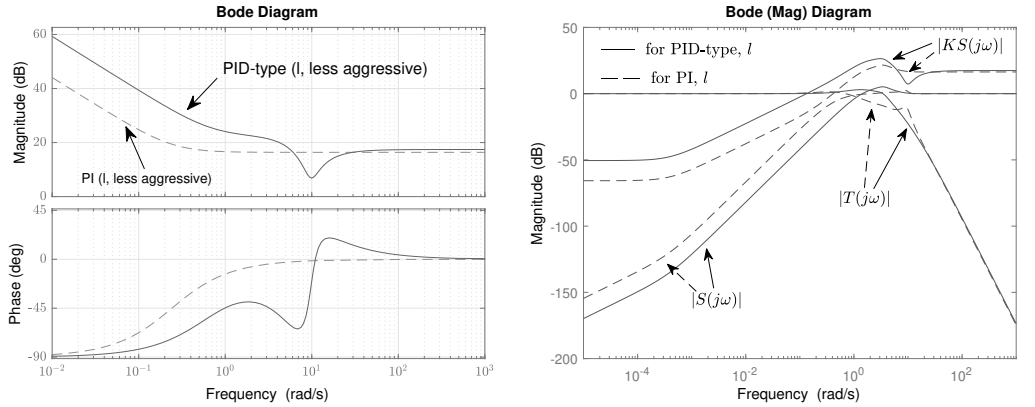

(a) Controller frequency response (b) Designed Closed loop frequency response

Figure 7: pv case: simple PI vs extended PID IMC-based control (design plant)

to be considered). Also, the simplified model gain is tuned to maintain the same amplitude peak for the retained resonant mode (nln case). The model approximation for the nulling-type design transfer function is

$$\tilde{G}_{\text{nln}}(s) = \frac{0.224\text{e}^{-\frac{s}{7.2}}}{s\left(1 + 0.037s + 0.01s^2\right)} \tag{22}$$

Figure 8 presents the frequency response of $G_{\text{nln}}(j\omega), \tilde{G}_{\text{nln}}(j\omega)$ for completeness. Using (22) and filter $F(s)$ of the form given by (20), the obtained nulling-type IMC controller will also be of the form given by (21), but will refer to it under controller id $C_{xPID-n}(s)$ for clarity (the PID-type controller is also listed in Appendix A). It is worth noting that in the nulling-type case IMC offers a direct way of incorporating the non-minimum phase zero constraint on control design by its mapping to a virtual time delay. Due to the control challenges for the nulling tilt case, only a PID-type controller is presented.

6. Results

The control strategies presented in this paper have been tested on a non-linear multi-body model of the complete vehicle. The equations of motion of the vehicle are written considering a rigid body schematisation for the carbody, the bogies and the wheelsets. Small displacements and rotation of

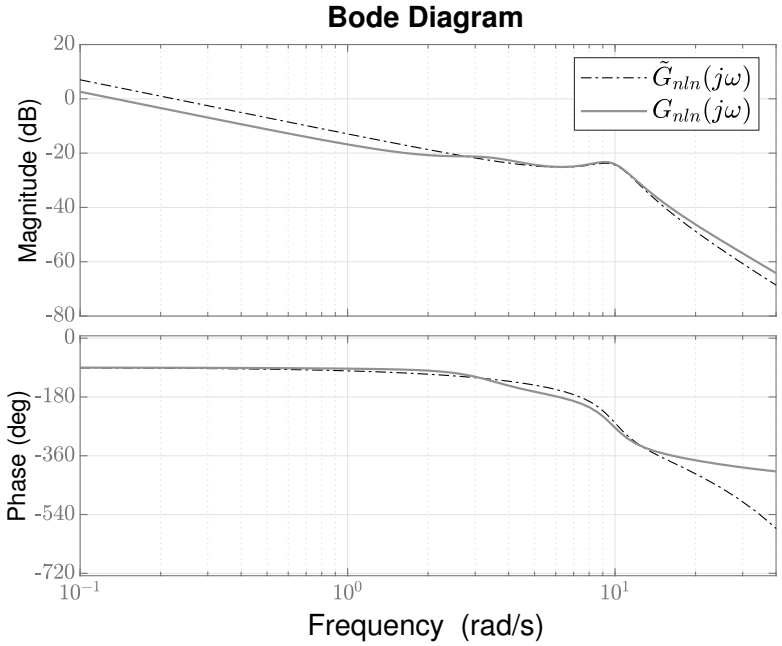

Figure 8: Plant transfer function $G_{\mathrm{nln}}(s)$ and its approximation

the bodies with respect to moving reference frames (following the track) are accounted for. In addition, a fully nonlinear description of the behaviour of suspension components (i.e. bumpstops etc.) and of the contact forces between the wheel and the rail is considered. More details on the multi-body software tool can be found in [19, 20, 21].

Three tilt control strategies have been adopted, the first two strategies on preview scheme, based on the knowledge of the track (by means of a geo-localisation system [53]), whereas the third is a nulling-type one with no preview information for completeness. All strategies implement IMC-based controllers, and for each of the schemes we investigate the effect of low and high aggressiveness controllers (subscripts "l", "h" indicate lower and higher aggressive control effort). The terms "low" and "high" aggressiveness, refer to more or less conservativeness in the speed of response.

Note that for the preview tilt implementation on the nonlinear MBS interface the feed-forward transfer-function was $\frac{A_{\mathrm{p}} b_{\mathrm{hyd}}}{k_{\mathrm{q}}} s(1+\tau_{\mathrm{f}} s)$ (essentially depicts the integrating actuator characteristics), with τ_{f} a small time-constant for approximate derivative (properness of the transfer function).

Firstly, time-domain simulations performed using an ideal deterministic

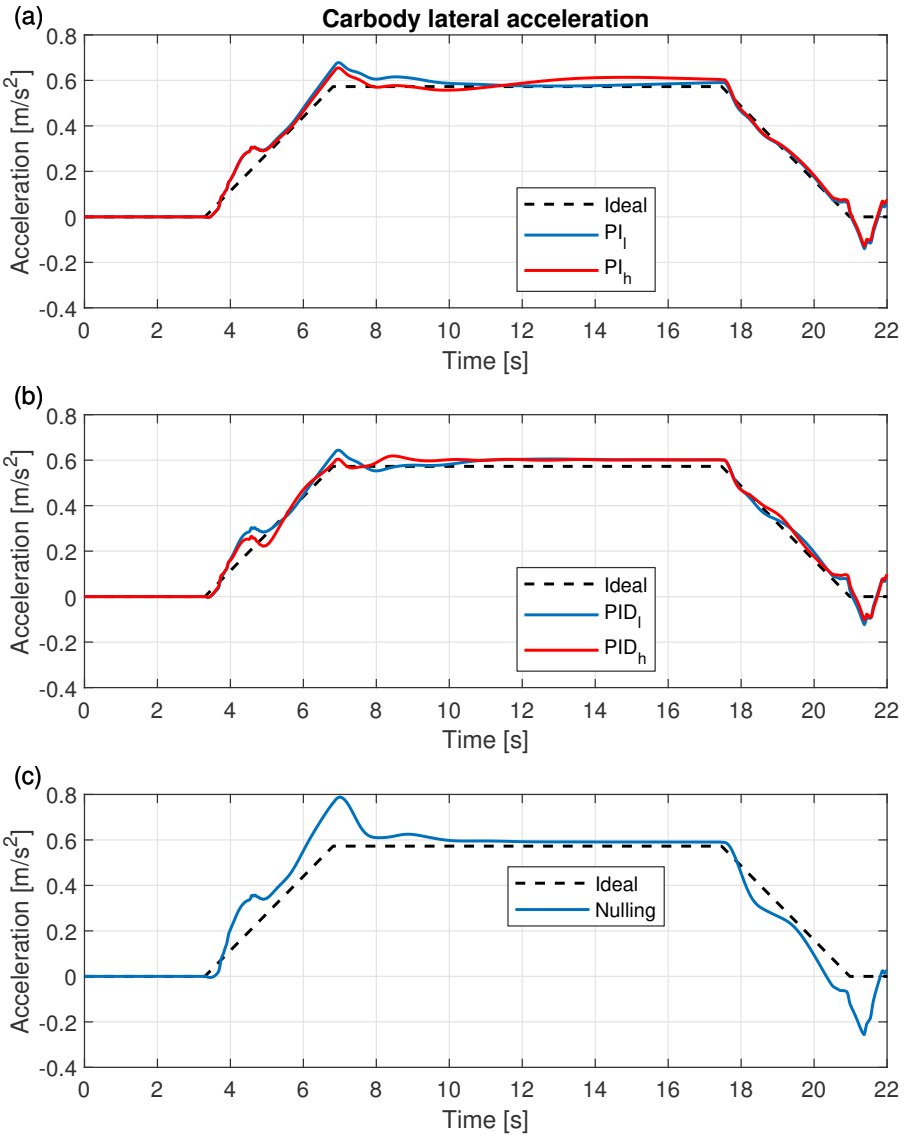

Figure 9: Carbody lateral acceleration: (a) PI, (b) extended PID; (c) Nulling (no track irregularities included to showcase the tracking aspect)

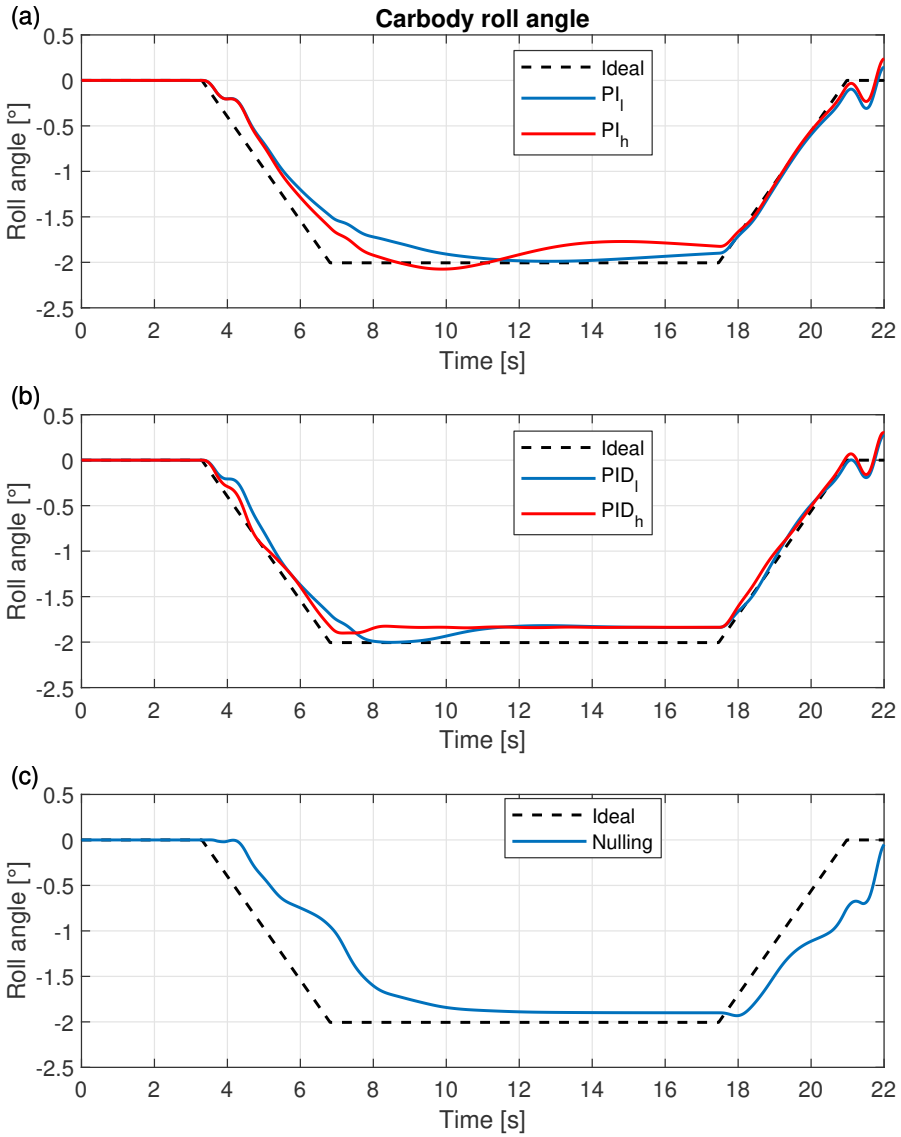

Figure 10: Carbody roll angle: (a) PI, (b) extended PID; (c) Nulling (no track irregularities included to showcase the tracking aspect)

track input (with no superimposed stochastic track irregularity and no sensor noise included) to analyse the quasi-static (tracking) behaviour of the controlled vehicle.

Figure 9 reports the carbody lateral acceleration profiles for the different controllers (excited by the track with no track irregularities imposed). In the figures the ideal compensated acceleration (no suspension interaction) is shown for completeness. The top figure, i.e. Figure 9 (a), presents the profiles obtained by PI controllers (no sensor noise has been included in order to showcase the signal profile clearly). It is observed that the less aggressive version (PI_l) exhibits slower settling response on account of its lower control gain. The more aggressive (PI_h) implementation settles quicker near the steady-state value. It is worth noting, as it will be observed also for the other controllers, the true steady-state value for the carbody lateral acceleration is not the one from the ideal profile but at slightly higher level due to the bogie roll-out (the multi-body software considers bogie dynamics in the simulation).

In the PID-type implementations, Figure 9 (b), there is similar trend in terms of the less and more aggressive controller behaviour. However, it is observed that the designed system exhibits faster settling time. Referring to the quasi-static performance of the nulling type control, see Figure 9 (c), it is observed that although the response is still acceptable it is also slower overall due to its non-preview nature (due to the natural feedback delay exhibited in the system, and cannot benefit from feed-forward action).

The carbody acceleration response trends are also supported by the relevant carbody roll angle response. PID-type implementations (Figure 10 (b)) exhibit faster settling time compared to PI (Figure 10 (a)) and nulling type (Figure 10 (c)) control. As the MBS tool includes realistic railway vehicle dynamics (including bogie), the bogie roll-out effect on steady state error is evident. It is worth noting that the nulling-type scheme is lesser affected by it (due to its "per-local-vehicle" information). Recall that the active carbody roll device is mounted between the bogie and the carbody, hence a torque is applied generating a relative carbody-bogie roll angle which can be estimated using actuators' displacements. Ideally, for zero steady-state roll and acceleration errors, the desired feedback signal for the controller is the carbody's absolute roll angle. However, the actual (measured) roll angle is that of carbody relative roll, which is affected by bogie roll-out. Although bogie roll-out is in principle small, cannot be negligible due to some primary suspension flexibility.

For completeness, a sample of the carbody acceleration profile excited by the combined rail track is also included, i.e. the response excited by both deterministic curved track and track irregularities imposed, shown on Figure 11 for the more aggressive controllers. It is shown that the proposed control schemes are not impacting stochastic performance of the tilt vehicle. It is also important to note that qualitatively the tilt control system will respond principally to the deterministic track inputs, while ignoring as much as possible any track irregularities.

Two different categories of parameters are evaluated, the first one related to passenger ride comfort, whereas the second category is associated to the controller performance (tracking, control effort). In particular in Table 2 we show the well-known PCT index as per the definition in [54]. This index is a weighted summation of the maximum values of the roll rate, the lateral acceleration and the lateral jerk and provides a measure of the passenger comfort in curve transitions (essentially the percentage of passengers that may experience nausea). In addition, the three different contribution on the PCT are reported together with the Root Mean Square (RMS) value of the lateral acceleration providing a global value of the lateral vibration felt by the passenger.

It is observed that derivative action in the controller facilitates reduction of PCT index level. For the nulling-type control approach the PCT index obtained is higher mainly due to the higher levels of maximum lateral acceleration and jerk (this is due to the naturally delayed roll angle response). However, the global RMS value of the lateral acceleration is only slightly larger than the other controllers. It is worth noting that the nulling-type controller does not benefit from preview information and therefore it reacts to the variation of lateral acceleration, thus generating a larger maximum lateral acceleration and jerk level. This is confirmed by the analysis of the performance of the different controllers, reported in Table 3, in particular by the maximum absolute error between the actual and ideal roll. The preview tilt PI and PID-type implementations are able to keep this value limited (to about 10.3 mrad), the nulling-type controller scheme exhibits a higher value i.e. approximately 19.5 mrad. From a power consumption viewpoint the RMS (of the power) required for performing the manoeuvre, evaluated for a single bogie, tends to increase in the PID-type implementation. In particular, the more aggressive implementation PID_h requires around 2.2 kW, while the less aggressive PID_l requires 1.6 kW (which is comparable to the PI controllers' value). It is worth noting that the nulling-type controller

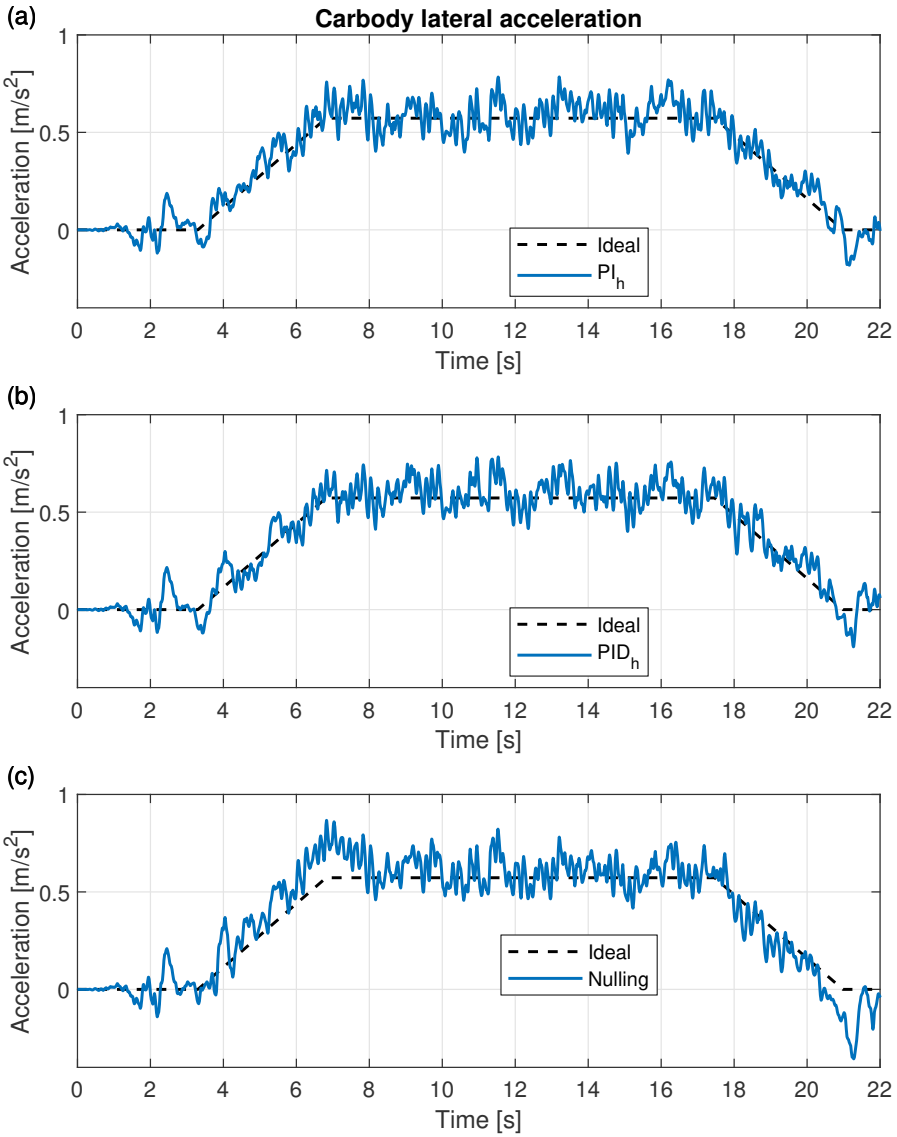

Figure 11: Carbody lateral acceleration: (a) PI, (b) extended PID; (c) Nulling (results with combined deterministic curved track and track irregularities)

imposes an intermediate RMS power value of 1.9 kW.

It is also seen that the designed controllers exhibit at least basic robust performance (as seen from the responses of the controllers implemented on the actual realistic nonlinear model on the MBS tool). It is recalled that the controllers were designed based on simplified linear (nominal) model versions of the actual vehicle, while frequency responses of the designed closed loop showcased early indication of robust performance as discussed in the previous sections.

Table 2: Evaluation of designed system comfort indices*

Controller	**Comfort evaluation**				
	P_{CT} [%]	$\max(\dot{\rho})$ [rad/s]	$\max(\ddot{y})$ [m/s^2]	$\max(\dddot{y})$ [m/s^3]	$RMS(\ddot{y})$ [m/s^2]
PI_l	2.468	**0.031**	0.664	0.217	0.195
PI_h	2.158	0.032	0.634	0.212	0.199
PID_l	**1.993**	0.033	0.619	**0.207**	**0.194**
PID_h	2.006	0.034	**0.599**	0.224	0.203
$Nulling$	3.465	**0.031**	0.740	0.251	0.204

* The simulation results consider the combined effect of deterministic curved track and random track irregularities.

Table 3: Evaluation of controller related performance*

Controller	**Control evaluation**		
	$\max\{\lvert\rho_{ref}-\rho\rvert\}$ [mrad]	$RMS(u)$ [V]	$RMS(Power)$ [kW]
PI_l	10.326	**0.047**	**1.436**
PI_h	8.391	0.050	1.546
PID_l	7.055	0.053	1.634
PID_h	**5.934**	0.071	2.194
$Nulling$	19.478	0.063	1.949

* The simulation results consider the combined effect of deterministic curved track and random track irregularities.

7. Conclusions

We have shown a structured process of modeling for control for the purposes of Internal Model Control (IMC) of rail carbody rolling in railway vehicles with hydraulic actuator dynamics. The presented IMC design enables simple PID type controllers. The presented study acts as a platform "bridging" ideas from PID-based process control to control of mechanical systems and provides a structured control design way that avoids complex optimization by tuning only a limited number of variables. The alternative nature of IMC design for the particular versions of preview-type and nulling-type tilt control design were highlighted. The paper clearly demonstrates high relevance to practical applications in control of railway vehicle structures, i.e. a theoretical control approach taking advantage of simple feedback setup for a complex railway vehicle control problem. It offers a valuable tool to leading-edge industrial rail control practitioners and applied researchers in the railway engineering sector. Preview tilt control offers better performance as it utilises tilt command reference, nulling-type tilt performance (while suffering from the well-known non-minimum phase zero and expected to be inferior to preview) is still at a relatively comparable level. The presented approach can be considered within the remit of a bank of controllers for fault tolerant carbody roll control purpose, or as a baseline controller to support further optimisation structured tilt controllers. Time-domain simulations were performed on an in-house railway Multi-Body Software tool at Politecnico di Milano implementing a realistic nonlinear railway vehicle model.

The following specific points are highlighted for the proposed IMC-based tilt controllers

(i) It forms a simple model based approach and, most importantly, does not necessitate complex optimization process;
(ii) It is the nature of IMC that enables fine loop-shaping with incorporation of higher order model approximations;
(iii) It provides a structured way of incorporating important plant modes for control design (as well as some dynamical performance constraints e.g. non-minimum phase zeros);
(iv) IMC-based tilt control performance can be comparable to state-based model-based schemes (for the latter the reader refers to [9]).

Current work looks into use of data-driven approaches in the control of the tilting vehicle system (emphasizing the use of the in-house software tool) and robust MIMO carbody roll control (i.e. using dual -lateral, roll - actuators).

References

[1] R. Persson, R. M. Goodall, K. Sasaki, Carbody tilting technologies and benefits, Vehicle System Dynamics 47 (8) (2009) 949–981.

[2] J. T. Pearson, R. M. Goodall, I. Pratt, Control system studies of an active anti-roll bar tilt system for railway vehicles, Proceedings of the Institution of Mechanical Engineers, Part F: Journal of Rail and Rapid Transit 212 (1) (1998) 43–60.

[3] Anon, SBB announces modernisation plans for 44 ICN tilting trains, Global Railway Review (2020 (accessed MArch 6, 2020)).
URL http://www.globalrailwayreview.com/news/97297/sbb-modernisation-plans-icn-tilting-trains/

[4] O. Fröidh, Perspectives for a future high-speed train in the swedish domestic travel market, Journal of Transport Geography 16 (4) (2008) 268 – 277.

[5] R. M. Goodall, T. X. Mei, Active suspension, in: Handbook of Railway Vehicle Dynamics, 2nd Edition, CRC Press, Boca Raton, FL, 2020.

[6] K. Tanifuji, S. Koizumi, R. Shimamune, Mechatronics in Japanese rail vehicles: active and semi-active suspensions, Control Engineering Practice 10 (9) (2002) 999–1004.

[7] Y. Nakakura, K. Hayakawa, The body inclining system of the series N700 Shinkansen, STECH'09 Conference, Niigata, Japan, 16-19 June 2009.

[8] A. Facchinetti, E. Di Gialleonardo, F. Resta, S. Bruni, V. Brundisch, Active control of secondary airspring suspension, Proceedings of the 22nd IAVSD Symposium, Manchester, UK, 14-19 August 2011.

[9] E. F. Colombo, E. Di Gialleonardo, A. Facchinetti, S. Bruni, Active carbody roll control in railway vehicles using hydraulic actuation, Control Engineering Practice 31 (2014) 24–34.

[10] H. Magalhães, P. Antunes, J. Pombo, J. A. Ambrósio, Dedicated control design methodology for improved tilting train performance, in: Advances in Dynamics of Vehicles on Roads and Tracks: Proceedings of

the 26th Symposium of the International Association of Vehicle System Dynamics, Springer, Springer, 2019, pp. 72–81.

[11] J. Förstberg, Ride comfort and motion sickness in tilting trains, Ph.D. thesis, Institutionen för farkostteknik (2000).

[12] S. Saxena, Y. V. Hote, Advances in internal model control technique: A review and future prospects, IETE Technical Review 29 (6) (2012) 461–472.

[13] M.-S. Chiu, Y. Arkun, Parametrization of all stabilizing imc controllers for unstable plants, International Journal of Control 51 (2) (1990) 329–340.

[14] D. E. Rivera, M. E. Flores, Internal model control, Control system, Robotics and Automation 2 (2009) 80–108.

[15] K. Zhou, A natural approach to high performance robust control: another look at youla parameterization, in: SICE 2004 Annual Conference, Vol. 1, 2004, pp. 869–874 vol. 1.

[16] D. S. Kumar, R. P. Sree, Tuning of IMC based PID controllers for integrating systems with time delay, ISA Transactions 63 (2016) 242–255. doi:10.1016/j.isatra.2016.03.020.
URL https://doi.org/10.1016/j.isatra.2016.03.020

[17] J. E. Arbogast, D. J. Cooper, Extension of IMC tuning correlations for non-self regulating (integrating) processes, ISA Transactions 46 (3) (2007) 303–311. doi:10.1016/j.isatra.2007.01.004.
URL https://doi.org/10.1016/j.isatra.2007.01.004

[18] K. Ghousiya Begum, A. Seshagiri Rao, T. Radhakrishnan, Enhanced imc based pid controller design for non-minimum phase (nmp) integrating processes with time delays, ISA Transactions 68 (2017) 223 – 234. doi:https://doi.org/10.1016/j.isatra.2017.03.005.

[19] S. Bruni, A. Collina, G. Diana, P. Vanolo, Lateral dynamics of a railway vehicle in tangent track and curve: Tests and simulation, Vehicle System Dynamics 33 (SUPPL.) (2000) 464–477.

[20] E. Di Gialleonardo, F. Braghin, S. Bruni, The influence of track modelling options on the simulation of rail vehicle dynamics, Journal of Sound and Vibration 331 (19) (2012) 4246–4258.

[21] S. Alfi, S. Bruni, Mathematical modelling of trainturnout interaction, Vehicle System Dynamics 47 (5) (2009) 551–574. doi:10.1080/00423110802245015.

[22] ERRI, B176 RP1 Bogies with steered or steering wheelsets, Volume 1: Preliminary studies and specifications, Volume 2: Specification for a bogie with improved curving characteristics, Volume 3: Specifications for a bogie with improved curving characteristics designed for body tilt, ERRI, Utrecht (1989).

[23] A. D. Rosa, S. Alfi, S. Bruni, Estimation of lateral and cross alignment in a railway track based on vehicle dynamics measurements, Mechanical Systems and Signal Processing 116 (2019) 606 – 623. doi:https://doi.org/10.1016/j.ymssp.2018.06.041.

[24] N. Zhang, W. A. Smith, J. Jeyakumaran, Hydraulically interconnected vehicle suspension: background and modelling, Vehicle System Dynamics 48 (1) (2010) 17–40. doi:10.1080/00423110903243182.
URL http://www.tandfonline.com/doi/abs/10.1080/00423110903243182

[25] H. Qi, N. Zhang, Y. Chen, B. Tan, A comprehensive tune of coupled roll and lateral dynamics and parameter sensitivity study for a vehicle fitted with hydraulically interconnected suspension system, Proceedings of the Institution of Mechanical Engineers, Part D: Journal of Automobile Engineering 235 (1) (2020) 143–161. doi:10.1177/0954407020944287.
URL https://doi.org/10.1177/0954407020944287

[26] G. Xu, N. Zhang, Characteristic analysis of roll and pitch independently controlled hydraulically interconnected suspension, SAE International Journal of Commercial Vehicles 7 (1) (2014) 170–176. doi:10.4271/2014-01-0870.
URL https://doi.org/10.4271/2014-01-0870

[27] S. Zhu, L. Wang, N. Zhang, H. Du, H∞ control of a novel low-cost roll-plane active hydraulically interconnected suspension: An experimental

investigation of roll control under ground excitation, SAE International Journal of Passenger Cars - Mechanical Systems 6 (2) (2013) 882–893. doi:10.4271/2013-01-1238.
URL https://doi.org/10.4271/2013-01-1238

[28] D. Allen, Active bumpstop hold-off-device, in: Proceedings of the IMechE conference Railtech, IMechE, 1994.

[29] H. E. Merritt, Robust Process Control, John Wiley & Sons, 1991.

[30] A. C. Zolotas, R. M. Goodall, G. Halikias, Recent results in tilt control design and assessment of high-speed railway vehicles, Proceedings of the Institution of Mechanical Engineers, Part F: Journal of Rail and Rapid Transit 221 (2) (2007) 291–312.

[31] L. A. Aguirre, Quantitative measure of modal dominance for continuous systems, in: Decision and Control, 1993., Proceedings of the 32nd IEEE Conference on, IEEE, 1993, pp. 2405–2410.

[32] A. Zolotas, G. Halikias, R. Goodall, J. Wang, Model reduction studies in lqg optimal control design for high-speed tilting railway carriages, in: American Control Conference, 2006, IEEE, 2006, pp. 6–pp.

[33] G. Lang, J. Ham, Conditional feedback systems-a new approach to feedback control, Transactions of the American Institute of Electrical Engineers, Part II: Applications and Industry 74 (3) (1955) 152–161.

[34] A. Faanes, S. Skogestad, Feedforward control under the presence of uncertainty, European Journal of Control 10 (1) (2004) 30–46.

[35] Q.-G. Wang, C. C. Hang, X.-P. Yang, Single-loop controller design via imc principles, Automatica 37 (12) (2001) 2041–2048.

[36] H. Bin, P. Zheng, J. Liang, Multi-loop internal model controller design based on a dynamic pls framework, Chinese Journal of Chemical Engineering 18 (2) (2010) 277–285.

[37] A. T. Azar, F. E. Serrano, Robust imc–pid tuning for cascade control systems with gain and phase margin specifications, Neural Computing and Applications 25 (5) (2014) 983–995.

[38] R. Vilanova, O. Arrieta, P. Ponsa, Imc based feedforward controller framework for disturbance attenuation on uncertain systems, ISA Transactions 48 (4) (2009) 439 – 448. doi:https://doi.org/10.1016/j.isatra.2009.05.007.

[39] A. K. Yadav, P. Gaur, Intelligent modified internal model control for speed control of nonlinear uncertain heavy duty vehicles, ISA Transactions 56 (2015) 288 – 298. doi:https://doi.org/10.1016/j.isatra.2014.12.001.

[40] J. Chen, Z.-F. He, X. Qi, A new control method for mimo first order time delay non-square systems, Journal of Process Control 21 (4) (2011) 538–546.

[41] R. De Keyser, C. Copot, A. Hernandez, C. Ionescu, Discrete-time internal model control with disturbance and vibration rejection, Journal of Vibration and Control 23 (1) (2017) 3–15.

[42] M. A. Henson, D. E. Seborg, An internal model control strategy for nonlinear systems, AIChE Journal 37 (7) (1991) 1065–1081.

[43] Z. Ping, T. Wang, Y. Huang, H. Wang, J.-G. Lu, Y. Li, Internal model control of pmsm position servo system: Theory and experimental results, IEEE Transactions on Industrial Informatics 16 (4) (2019) 2202–2211.

[44] D. E. Rivera, M. Morari, Internal model control perspectives on model reduction, in: 1985 American Control Conference, 1985, pp. 1293–1298. doi:10.23919/ACC.1985.4788818.

[45] S. Skogestad, Simple analytic rules for model reduction and pid controller tuning, Journal of process control 13 (4) (2003) 291–309.

[46] A.-V. Duka, M. Dulău, S.-E. Oltean, Imc based pid control of a magnetic levitation system, Procedia Technology 22 (2016) 592–599.

[47] M. Canale, L. Fagiano, Stability control of 4ws vehicles using robust imc techniques, Vehicle System Dynamics 46 (11) (2008) 991–1011.

[48] M. Canale, L. Fagiano, A. Ferrara, C. Vecchio, Comparing internal model control and sliding-mode approaches for vehicle yaw control, IEEE Transactions on Intelligent Transportation Systems 10 (1) (2009) 31–41. doi:10.1109/TITS.2008.2006772.

[49] T. N. Vu, D. V. Dung, N. V. Trang, P. T. Hai, Analytical design of PID controller for enhancing ride comfort of active vehicle suspension system, 2017 International Conference on System Science and Engineering (ICSSE) (2017) 305–308.

[50] T.-L. Chia, I. Lefkowitz, Internal model-based control for integrating processes, ISA transactions 49 (4) (2010) 519–527.

[51] D. Chen, D. E. Seborg, Pi / pid controller design based on direct synthesis and disturbance rejection, Industrial & engineering chemistry research 41 (19) (2002) 4807–4822.

[52] E. Zafiriou, M. Morari, Robust Process Control, Prentice-Hall International, 1989.

[53] H. Higaki, S. Fuiimori, Y. Horike, T. Yasui, S. Koyanagi, I. Okamoto, K. Terada, An active pneumatic tilting system for railway cars, Vehicle System Dynamics 20 (sup1) (1992) 254–268.

[54] CEN, EN 12299:Railway Applications Ride Comfort for Passengers Measurement and Evaluation, CEN, Brussels (April 2009).

Appendix A. IMC-based controllers

Controller TF presented in LTI continuous-time form. Also note that, in PID-type controllers, the ideal PID portion is shown using **boldface font**.

*Appendix A.1. Preview (*pv*)*

PI-type (more aggressive response):

$$C_{\text{xPI-h}}(s) = \frac{5.8569(1.125s + 1)}{s} \tag{A.1}$$

PI-type (less aggressive response):

$$C_{\text{xPI-l}}(s) = \frac{1.5973(4.125s + 1)}{s} \tag{A.2}$$

PID-type (less aggressive response):

$$C_{\text{xPID-l}}(s) = \frac{\mathbf{7.4424}(s + 0.6906)(\mathbf{s^2 + 3.625s + 96.12})}{\mathbf{s}(s^2 + 11.43s + 53.61)} \tag{A.3}$$

PID-type (more aggressive response):

$$C_{\text{xPID-h}}(s) = \frac{\mathbf{345.54}(s+2.232)(\mathbf{s^2+3.625s+96.12})}{\mathbf{s}(s^2+40s+815)} \tag{A.4}$$

Remark on (IMC) PID-type controller structure: For the plant choice (19) and filter choice (20), and taking $\tau_0 = n \times \tilde{\theta}$ $(n \geq 1)$, the following are noted (symbolic analysis). The controller structure is given, after some extensive calculations, by

$$C_{\text{PID-type}}(s) = \boxed{(k'\tilde{\theta}^2)^{-1}} \frac{\big(1+s\tilde{\theta}\,(1+4n)\big)\,\boxed{(1+2\xi_2\tau_2 s+(\tau_2 s)^2)}}{\boxed{s}\big(n^4(\tilde{\theta}s)^2+4n^3\tilde{\theta}s+(6n^2+4n+1)\big)} \tag{A.5}$$

It can be clearly seen that the PID portion of the controller above, (A.5) (boxed elements), is mainly defined by the approximated plant dynamics used for the design, while the effective delay scales its gain. The low-pass shaper is governed by the filter selection. Similar analysis follows for the nulling tilt design aspect. (Some controller de-tuning can be followed if necessary, as is the case in many practical applications, for further refinement of performance.)

For completeness, Figure A.12, illustrates the contributions of the PID portion and the lowpass shaper on the overall PID-type controller (less aggressive case for preview tilt).

*Appendix A.2. Nulling (*nln*)*

PID-type (balanced response, deterministic/stochastic):

$$C_{\text{xPID-n}} = \frac{\mathbf{1.4369}(s+0.3752)(\mathbf{s^2+3.625s+96.12})}{\mathbf{s}(s^2+6.504s+19.68)} \tag{A.6}$$

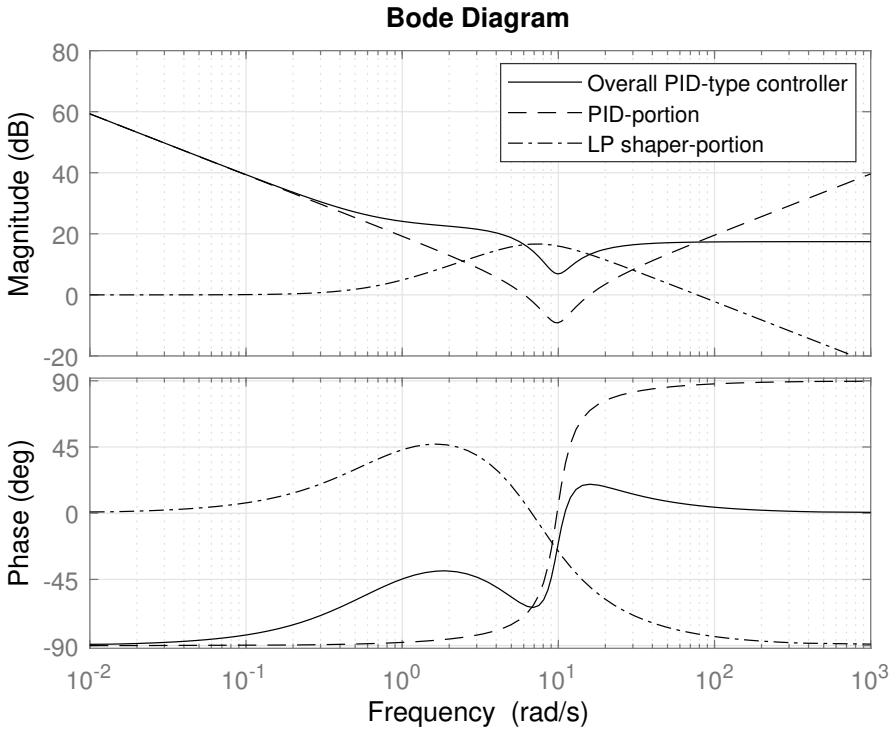

Figure A.12: PID-type (preview tilt, less aggressive) bode plot

Appendix B. Matrices for state space formulation and parameter values

$$[A] = \begin{bmatrix} -\frac{c_\mathrm{l}}{m} & -\frac{c_\mathrm{l} h_\mathrm{cl}}{m} & -\frac{k_\mathrm{l}}{m} & \frac{k_\mathrm{l} h_\mathrm{kl}}{m} & 0 & 0 \\ \frac{c_\mathrm{l} h_\mathrm{cl}}{J} & -\frac{1}{J}\left(c_\mathrm{l} h_\mathrm{cl}^2 + 2c_\mathrm{v}\frac{b_\mathrm{cv}^2}{4}\right) & \frac{k_\mathrm{l} h_\mathrm{kl}}{J} & -\frac{1}{J}\left(k_\mathrm{l} h_\mathrm{kl}^2 + 2k_\mathrm{v}\frac{b_\mathrm{kv}^2}{4}\right) & \frac{b_\mathrm{hyd} A_\mathrm{p}}{J} & 0 \\ 1 & 0 & 0 & 0 & 0 & 0 \\ 0 & 1 & 0 & 0 & 0 & 0 \\ 0 & -\frac{\beta}{V_0} b_\mathrm{hyd} A_\mathrm{p} & 0 & 0 & -\frac{\beta}{V_0}\left(2C_\mathrm{i} + C_\mathrm{e} + k_\mathrm{c}\right) & \frac{\beta}{V_0} k_\mathrm{q} \\ 0 & 0 & 0 & 0 & 0 & -\frac{1}{\tau_\mathrm{s}} \end{bmatrix}$$

$$[B_u] = \begin{bmatrix} 0 \\ 0 \\ 0 \\ 0 \\ 0 \\ \frac{1}{\tau_\mathrm{s}} \end{bmatrix}$$

$$[B_w] = \begin{bmatrix} v^2 & 0 & 0 & 0 & -g \\ -\frac{mv^2}{J} h_\mathrm{lat} & -\frac{c_\mathrm{l} h_\mathrm{cl}}{J} & \frac{1}{J}\left(c_\mathrm{l} h_\mathrm{cl}^2 + 2c\frac{b_\mathrm{cv}^2}{4}\right) & -\frac{k_\mathrm{l} h_\mathrm{kl}}{J} & \frac{mg}{J} h_\mathrm{lat} \\ 0 & 0 & 0 & 0 & 0 \\ 0 & 0 & 0 & 0 & 0 \\ 0 & 0 & 0 & 0 & 0 \\ 0 & 0 & 0 & 0 & 0 \end{bmatrix}$$

Table B.1: Vehicle parameters

Parameter	Description	Value	u.m.
m	Carbody mass	20366	kg
J	Roll inertia	44000	kgm^2
c_v	Vertical damping	13000	$\frac{Ns}{m}$
c_l	Lateral damping	65000	$\frac{Ns}{m}$
k_l	Lateral stiffness	248000	$\frac{Ns}{m}$
k_v	Airspring vertical stiffness	300000	$\frac{N}{m}$
b_{cv}	Vertical damper spacing	2.57	m
b_{kv}	Airspring spacing	2	m
h_{cl}	Lateral damping height	1.23	m
h_{kl}	Lateral spring height	1.28	m
h_{lat}	Active lateral suspension height	1.35	m

Table B.2: Active anti-roll device parameters

Parameter	Description	Value	u.m.
V_{res}	Volume of each reservoir	$1.5 \cdot 10^{-2}$	m^3
y_{max}	Maximum piston stroke	0.24	m
A_p	Piston area	$1.963 \cdot 10^{-3}$	m^2
V_0	Half of the vol. of each branch in the circuit	$8 \cdot 10^{-3}$	m^3
C_i	Internal leakage coefficient	10^{-14}	$\frac{m^3}{Pa}$
C_e	External leakage coefficient	0	$\frac{m^3}{Pa}$
β	Oil bulk modulus	$1.1 \cdot 10^9$	Pa
P_s	Supply pressure	198	bar
P_r	Return pressure	2	bar
b_{hyd}	Distance between actuators	2.57	m